p-ISSN 2089 – 0133 e-ISSN 2477-6416
URL : https://jurnal.uns.ac.id/ijap/article/view/114864

Indonesian Journal of Applied Physics (IJAP) Vol. 16 No. 1 page 62
DOI : https://doi.org/10.13057/ijap.v16i1.114864

NUMERICAL TSUNAMI HAZARD MODELLING IN THE PANCER COAST - PUGER, EAST JAVA, INDONESIA

Rozikan [1,2], Agus Supriyanto*[3], M. Aryono Adhi[4], Bowo Eko Cahyono[3]

[1]Magister of Physics, Faculty of Mathematics and Natural Sciences, University of Jember, Indonesia
[2] Geophysics Station of Pasuruan, Indonesian Agency for Meteorology, Climatology, and Geophysics (BMKG), Pandaan, Pasuruan, Indonesia
[3] Physics Department, Faculty of Mathematics and Natural Sciences, University of Jember, Jember, Indonesia
[4] Physics Department, Faculty of Mathematics and Natural Science, Semarang State University, Indonesia
* a_suprianto.fmipa@unej.ac.id

Received 2026-01-19, Revised 2026-04-23, Accepted 2026-06-02,
Available Online, Published Regularly June 2026

ABSTRACT

The southern Java subduction zone is one of the major tsunami hazard sources in Indonesia due to its potential to generate large megathrust earthquakes. This study evaluates tsunami hazards from a Mw 8.7 megathrust earthquake worst-case scenario using numerical modeling with COMCOT v1.7. A five-layer nested grid system is applied to simulate tsunami generation, propagation, and inundation from the Indian Ocean to the Pancer - Puger coast, Jember Regency, Indonesia. Earthquake source parameters are defined using the Wells and Coppersmith empirical relationships, while initial seafloor deformation is calculated using the Okada elastic dislocation model. Tsunami wave dynamics are analyzed using Virtual Tsunami Gauges (VTGs). The results indicate that Puger Kulon and Mojosari villages experience the most severe impacts, with large wave amplitudes, strong currents, and inundation exceeding 20 m depths. Tsunami arrival time is about 21 to 27 minutes, providing a very limited evacuation window. The ETH (Estimated Tsunami Height) and ETA (Estimated Time of Arrival) maps show that low-lying, open coastal plains act as primary pathways for tsunami penetration. These findings emphasize the high vulnerability of the Pancer coast - Puger and the need for risk-based mitigation, improved evacuation planning, and strengthened local early warning systems.

Keywords: tsunami; COMCOT; Pancer coast; inundation; arrival time

INTRODUCTION

Indonesia is one of the most seismotectonically active regions in the world, as it is located at the convergence of four major tectonic plates: the Indo-Australian, Eurasian, Pacific, and Philippine plates. The interaction among these plates has formed 16 subduction zones and 13 megathrust segments, which are capable of generating large earthquakes accompanied by destructive tsunamis [1-5]. Along the southern coast of Java, including East Java, the subduction of the Indo-Australian Plate at a convergence rate of approximately 6–7 cm/year leads to the accumulation of tectonic energy that may be released in the form of large-magnitude megathrust earthquakes [6-7]. Historical events, such as the 1994 Banyuwangi tsunami and the 2006 Pangandaran tsunami, demonstrate that major earthquakes in this zone can generate tsunamis with significant coastal impacts [5,8-9]. The Pancer–Puger area in Jember Regency was affected during the 1994 event, further emphasizing its classification as a coastal region with a high level of tsunami risk.

Based on the Spatial Planning Regulation (RTRW) of Jember Regency, the coastal area of Pancer-Puger is classified as a tsunami-prone zone, which is reinforced by the high concentration of settlements and fisheries-related activities along the coastline [10]. In addition, the Indonesian Disaster Risk Index (IRBI) classifies Jember Regency as a high-risk area for tsunami hazards [11]. The InaRISK data published by the National Disaster Management Agency (BNPB) in 2024 [12] also indicates that Jember Regency is considered the highest tsunami risk area in East Java, highlighting the urgent need for a more comprehensive and quantitative tsunami risk assessment [13-14]. The numerical tsunami modeling is capable of quantitatively describing the potential tsunami impacts in the Pancer-Puger area.

Previous studies on tsunami potential along the southern coast of Java have been conducted using geodetic and seismotectonic approaches, as well as numerical tsunami modeling with various models such as COMCOT, MOST, and TUNAMI-N2 [5, 15-21]. These studies provide a general overview of megathrust source characteristics and tsunami run-up potential in several coastal regions of Indonesia. However, no study has specifically simulated a megathrust earthquake scenario with a magnitude of Mw 8.7 and analyzed its detailed impacts in the Pancer–Puger area, particularly in terms of tsunami arrival time (Estimated Time of Arrival/ETA), inundation depth distribution (Estimated Tsunami Height/ETH), and variations in local responses influenced by site-specific geomorphological characteristics [14],[22] .

Based on this research gap, this study aims to analyze tsunami impacts in the Pancer coastal - Puger area, Jember Regency, under a deterministic Mw 8.7 megathrust worst-case scenario based on PuSGeN (2017) [3]. The analysis focuses on ETA, inundation height and spatial distribution of ETH, as well as wave propagation characteristics from the source region to the coast [19-21]. The results of this study are expected to provide more accurate quantitative insights into tsunami hazard levels in the Pancer coast - Puger area and to serve as a scientific basis for strengthening local-scale tsunami mitigation strategies [21-22].

METHOD

This study was conducted in the Pancer–Puger Kulon coastal area, Puger District, Jember Regency, which is located directly in front of the southern Java subduction zone. The datasets used for tsunami modeling include GEBCO bathymetry [23], BATNAS, and DEMNAS topographic data (Geospatial Information Agency [BIG] 2018) [24]. In addition, land cover data from the Ministry of Environment and Forestry (KLHK) were used to assign Manning's roughness coefficients (n), representing variations in surface resistance during tsunami propagation from offshore to onshore environments [17, 25-26]. The land-use classification was further refined using recent Google Earth imagery to better represent current coastal conditions.

The Manning roughness coefficient was implemented in the COMCOT model using the variable friction option (Var.n), allowing different surface characteristics such as vegetation, built-up areas, and open land to influence flow resistance, velocity, and inundation extent, consistent with established numerical tsunami modeling approaches [27].

To ensure a systematic and integrated modeling procedure, the research was carried out through a structured methodological framework covering data preparation, earthquake source characterization, tsunami simulation, and result analysis. The overall research workflow is summarized in Figure 1, which illustrates the logical sequence and interconnection of the main stages in COMCOT-based tsunami modeling.

Figure 1. Research workflow of COMCOT-based tsunami modeling, illustrating the main stages from data preparation, megathrust earthquake source modeling, nested-grid tsunami simulation, to the analysis of ETA) and ETH in the Pancer coastal - Puger area, Jember Regency, Indonesia.

The tsunami source was modeled using a megathrust earthquake scenario with a moment magnitude of Mw 8.7, based on the Indonesian Earthquake Source and Hazard Map [3]. The source was represented by three fault segments (A, B, and C), as shown in Figure 2, following the geometry of the southern Java megathrust. Fundamental fault parameters, including fault length and width, were estimated using the empirical relationships proposed by Wells & Coppersmith (1994) [28], which relate earthquake magnitude to fault dimensions through logarithmic scaling, as expressed in Equations (1) and (2).

$$log\, L = a_1 + b_1 M_w \tag{1}$$

$$log\, W = a_2 + b_2 M_w \tag{2}$$

where L denotes fault length (km), W is fault width (km), a_1 and a_2 are empirical constants associated with fault dimensions, b_1 and b_2 are regression coefficients relating magnitude to rupture dimensions, and Mw is earthquake moment magnitude.

The average slip (D) was estimated using the seismic moment formulation, which relates the seismic moment (M_0) to the shear modulus (μ) and the fault rupture area (A), as expressed in Equation (3). The seismic moment was first calculated from the moment magnitude (Mw) using the empirical relationship proposed by Kanamori (1977) [29], as presented in Equation (4).

$$M_0 = \mu A D \tag{3}$$

$$M_w = \frac{2}{3}(log\, M_0 - 9.1) \tag{4}$$

where M_0 is seismic moment (N·m), μ denotes crustal shear modulus, assumed to be 3.0×10^{10} Pa, A is the fault rupture area, D is average fault slip (m), and Mw is moment magnitude.

Based on the Mw 8.7 megathrust earthquake scenario adopted in this study, fault parameters, including fault length, width, depth, strike, dip, rake, and slip, were determined for each fault segment and implemented as input parameters in the tsunami simulations. The complete set of fault parameters is summarized in Table 1.

Table 1. Fault parameters of the Mw 8.7 megathrust earthquake scenario used in the tsunami simulation.

Id_fault	*Lon (°)*	*Lat (°)*	*fault_P (km)*	*fault_L (km)*	*Depth (km)*	*strike (m)*	*Dip (°)*	*Slip (°)*	*Dislocation (m)*
A	111.1926	-9.99970	141000	91000	20000	275	10	90	19
B	112.4832	-10.1723	141000	91000	17000	280	7	90	19
C	113.7619	-10.4503	141000	91000	18000	285	9	90	19

Seafloor deformation generated by the displacement of the three fault segments was calculated using the elastic dislocation formulation of Okada (1985) [30] to produce a two-dimensional uplift subsidence pattern. The resulting vertical deformation was then applied as the initial water surface displacement in the COMCOT tsunami model, which is a standard approach in earthquake-generated tsunami simulations [27].

Tsunami propagation and inundation were simulated using a nested grid system consisting of five computational domains (Layer 01- 05), allowing the tsunami dynamics to be captured from the regional Indian Ocean scale to the local coastal scale of Pancer - Puger. The nested grid configuration and the location of the three megathrust fault segments are shown in Figure 2.

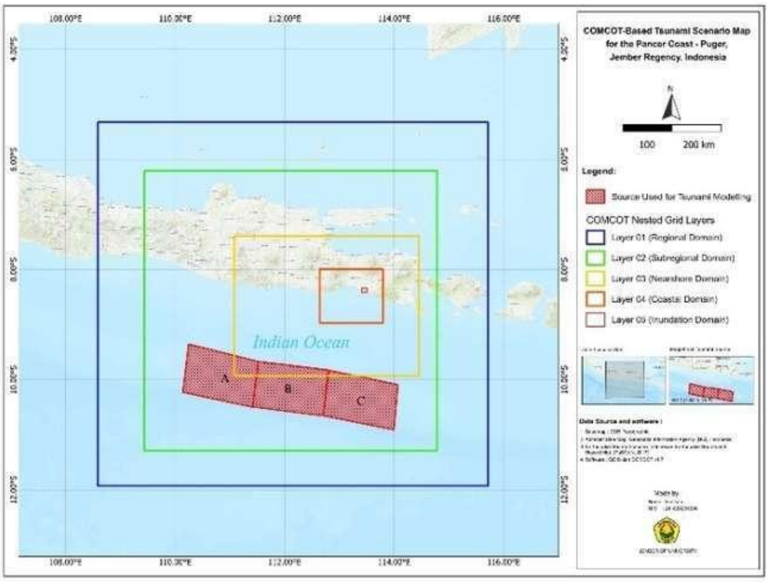

Figure 2. COMCOT-based tsunami scenario map showing the nested grid configuration and segmented megathrust earthquake source (segments A, B, and C) used for tsunami simulations along the Pancer coast - Puger, Jember Regency, Indonesia.

The nested grid approach is widely used in tsunami modeling to combine extensive spatial coverage with high-resolution coastal representation [17],[31]. Offshore domains were simulated using coarser grid resolutions, while nearshore and onshore areas were represented with finer grids. This strategy enables realistic tsunami propagation from the megathrust source to coastal inundation while maintaining computational efficiency. The coordinate boundaries of each modelling layer are provided in Table 2.

Table 2. Configuration of the COMCOT tsunami modeling domains

Layer	X, Y Start	X, Y End
1	108.6, -11.91	115.72, -5.34
2	109.47, -11.27	114.81, -6.24
3	111.09, -9.94	114.47, -7.44
4	112.64, -8.99	113.82, -8.09
5	113.394, -8.416	113.506, -8.321

Tsunami simulations were performed using COMCOT version 1.7, which solves the Nonlinear Shallow Water Equations (NSWE) to represent tsunami generation, propagation, and inundation processes [32]. The tsunami dynamics are governed by the continuity equation (Equation 5), which expresses mass conservation [31]:

$$\frac{\partial \eta}{\partial t} + \frac{\partial M}{\partial x} + \frac{\partial N}{\partial x} = 0 \tag{5}$$

where η denotes the sea surface elevation, Mand Nare the depth-integrated flow fluxes in the x- and y-directions, respectively, and t represents time.

The tsunami flow dynamics are governed by the principle of momentum conservation. In the x-direction, the momentum conservation equation is expressed by Equation (6) [17]:

$$\frac{\partial M}{\partial t}+\frac{\partial}{\partial x}(\frac{M^2}{D}+\frac{1}{2}gD^2)+\frac{\partial}{\partial y}(\frac{MN}{D})=-gD\frac{\partial h}{\partial x}-\tau_x \tag{6}$$

with an analogous equation applied in the y-direction. In these equations, $D=h+\eta$ represents the total water depth, h is the bathymetric depth, g is gravitational acceleration, and τ_x denotes the bottom friction term, parameterized using Manning's roughness coefficient. The governing equations were solved numerically using a finite-difference scheme to obtain the temporal evolution of sea surface elevation, flow velocity, and tsunami energy distribution across all modeling layers.

Virtual Tsunami Gauge Point

Virtual Tsunami Gauges (VTGs) were employed in this study to record tsunami wave characteristics at selected locations along the southern coast of Jember. VTGs function as virtual measurement points within the COMCOT numerical domain, recording time-dependent variations in sea surface elevation and flow velocity [17],[31].

A total of four VTGs were deployed at Pancer Beach (Jember), Nusa Barung Island (Jember), Watu Gedek Beach (Lumajang), and Lampon Beach (Banyuwangi), as shown in Figure 3. The gauges were positioned near the coastline to capture shoaling processes, wave transformation, and nearshore amplification prior to coastal inundation [27].

The VTG outputs, consisting of wave amplitude and current velocity components, were analyzed to determine the Estimated Time of Arrival (ETA) and to assess spatial variations in tsunami energy at each observation site.

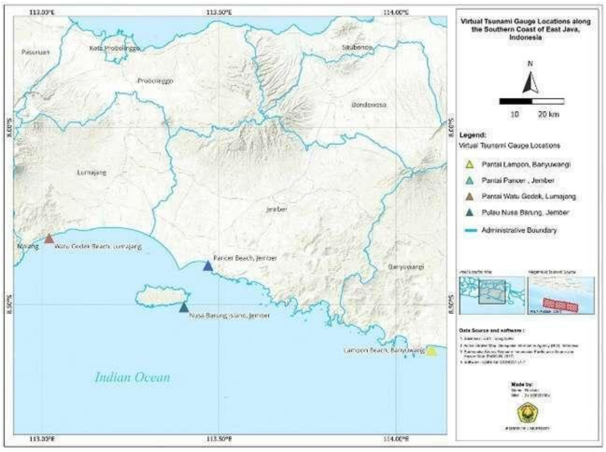

Figure 3. Virtual Tsunami Gauge locations along the southern coast of East Java

RESULTS AND DISCUSSION

Seafloor Deformation

Figure 4 illustrates the pattern of initial water surface displacement generated by the Mw 8.7 megathrust earthquake scenario using COMCOT version 1.7, with visualization performed in GNU Octave 9.2.0. The deformation pattern results from the displacement of three fault segments computed using the elastic dislocation formulation of Okada (1985) [30], producing zones of uplift (yellow-green) and subsidence (purple–blue) that extend parallel to the geometry of the southern Java subduction zone.

The maximum uplift reaches approximately +6 m, while subsidence attains about -4 m, reflecting the magnitude of slip and source dimensions that are consistent with the empirical magnitude-fault scaling relationships proposed by Wells & Coppersmith (1994) [28]. These deformation magnitudes are generally consistent with those expected for an Mw 8.7 megathrust event and indicate substantial coseismic seafloor displacement capable of generating significant tsunami waves. Positive uplift contributes to the initial displacement of the water column and tsunami generation, whereas subsidence influences wave propagation patterns and associated coastal hazard levels. This pattern indicates the influence of the southern Java megathrust geometry on the initial direction of tsunami energy generation, as also demonstrated by recent seismotectonic and tsunami modeling studies in southern Java [3,5, 26-27, 33].

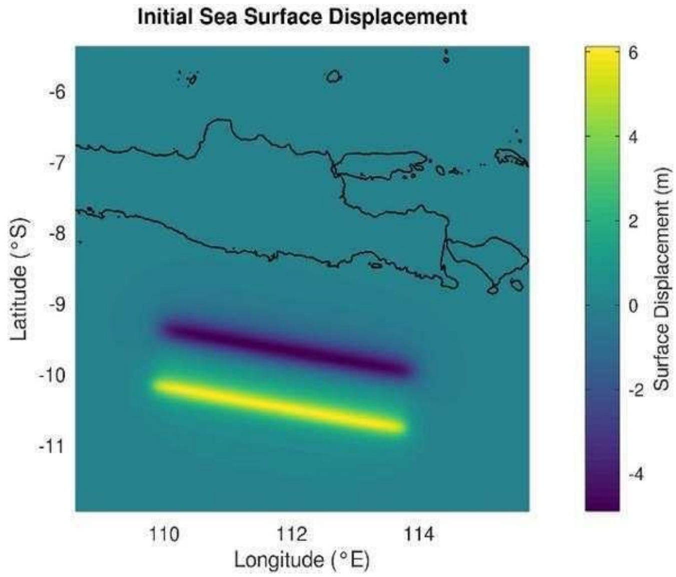

Figure 4. Initial sea surface displacement generated by an Mw 8.7 megathrust earthquake simulated using COMCOT. The color scale represents vertical sea surface displacement (m), ranging from approximately −4 m (maximum subsidence) to +6 m (maximum uplift). Positive values (yellow-green) indicate uplift, while negative values (blue-purple) indicate subsidence.

The computed seafloor deformation, transferred as the initial sea surface displacement, was applied as the initial condition in tsunami propagation simulations within the nested grid system, thereby playing a critical role in controlling the dominant propagation direction, initial tsunami amplitude, and the overall early-stage tsunami generation process [17],[27],[31].

Tsunami Wave Generation

The maximum tsunami amplitude modeling results illustrate the evolution of the initial deformation caused by the Mw 8.7 megathrust earthquake into fully developed tsunami waves propagating across the southern Indian Ocean off Java (Figure 5). The spatial distribution of maximum amplitude represents the transformation of initial uplift–subsidence of the seafloor into propagating tsunami energy in the open ocean.

Near the source region, the maximum tsunami amplitude retains the geometric imprint of the fault segments, reaching values exceeding 15 m. This zone corresponds to the highest energy release directly associated with the initial sea surface displacement. With increasing distance from the source, tsunami amplitudes gradually decrease due to energy dispersion and dissipation during wave propagation.

As the tsunami waves approach the southern coast of East Java, maximum amplitudes increase markedly due to shoaling and coastal focusing effects. Although offshore amplitudes are generally in the range of 3–6 m, nearshore amplitudes become strongly amplified along the Pancer-Puger coastline, locally exceeding 10 m in several coastal segments (Figure 5). The highest concentrations of tsunami amplitude occur near Pancer and Puger, where shallow nearshore bathymetry and embayed coastal geometry enhance wave amplification and energy focusing prior to landfall. Spatial variability along the coast indicates that sectors directly exposed to the incoming tsunami wavefront exhibit larger amplitudes than adjacent coastal segments, while localized amplification hotspots are observed particularly along the Pancer embayment and the Puger coastal sector, reflecting the influence of bathymetric irregularities and shoreline orientation, consistent with previous tsunami modelling studies in active subduction zones [5],[17],[26],[34].

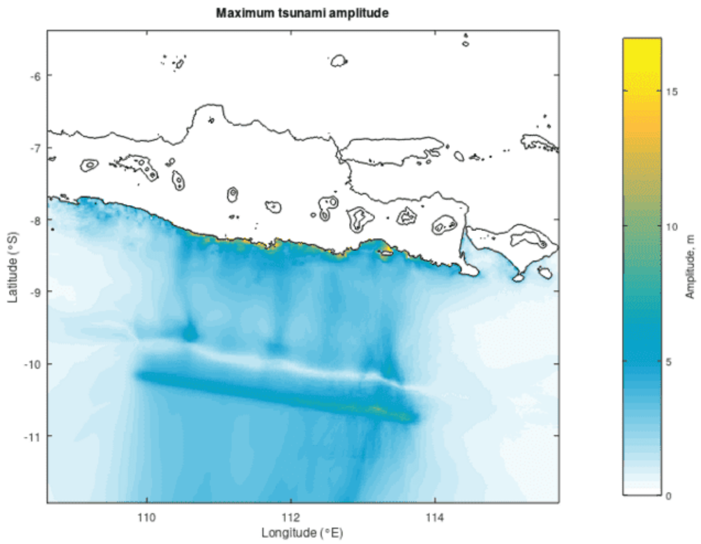

Figure 5. Maximum tsunami wave amplitude generated by the Mw 8.7 megathrust earthquake scenario simulated using COMCOT. The color scale indicates modeled maximum wave amplitude (m), highlighting high amplitudes near the source region and localized amplification along the Pancer-Puger coast.

Tsunami Propagation

The temporal evolution of tsunami propagation from 0 to 60 minutes after the initial deformation is illustrated by a sequence of model snapshots (Figure 6a–d). The color scale represents instantaneous sea surface elevation (η, in meters), where positive values indicate wave crests and negative values indicate troughs. At 0 minutes, the uplift–subsidence pattern dominates, representing the initial wave generation stage above the source region. By 15 minutes, tsunami waves begin to radiate away from the source, forming a radial propagation pattern toward the southern coast of Java. At 30 minutes, the leading wave front enters shallow coastal waters and undergoes shoaling and amplitude amplification. By 60 minutes, the wave field becomes more complex, reflecting interactions between incoming and reflected waves that produce interference patterns controlled by local bathymetry and coastal geometry.

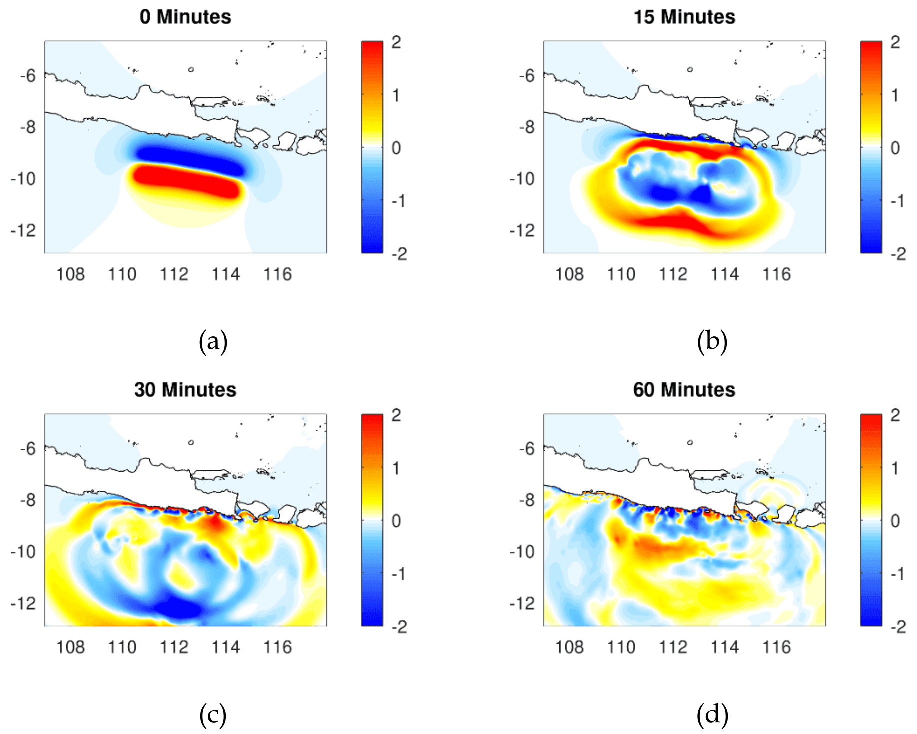

Figure 6. Snapshots of tsunami wave propagation at (a) 0, (b) 15, (c) 30, and (d) 60 minutes after the initial seafloor deformation. The color scale represents instantaneous sea surface elevation (m), ranging from −2 m (blue, trough) to +2 m (red, wave crest), illustrating the temporal evolution of wave propagation and amplification.

Overall, the simulation results indicate that tsunami energy is preferentially focused toward the southern coast of East Java, including the Pancer - Puger area, with wave amplification strongly controlled by seafloor morphology and water depth. This propagation is characteristic of megathrust-generated tsunamis in active subduction zones, where significant vertical seafloor deformation plays a primary role in tsunami generation and coastal impact [26],[27],[35].

Virtual Tsunami Gauge (VTG)

The temporal characteristics of tsunami waves were analyzed using four Virtual Tsunami Gauges (VTGs) representing key coastal settings along the southern coast of East Java, namely Pancer Beach (Jember), Nusa Barung Island (Jember), Watu Gedek Beach (Lumajang), and Lampon Beach (Banyuwangi). The selection of VTG locations was based on their proximity to the tsunami source, coastal morphology, and west–east spatial distribution of the study area [26,36-37]. The spatial distribution of the VTGs is shown in Figure 7, while the time series of water surface elevation and current velocity are presented in Figures 8(a–d).

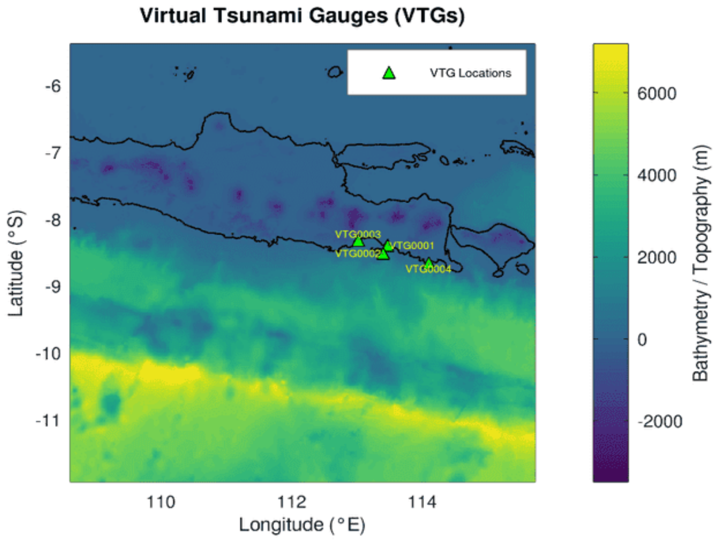

Figure 7. Locations of the Virtual Tsunami Gauges (VTGs) used in the COMCOT simulation. Triangles indicate the four VTG monitoring points along the southern coast of East Java. The background color scale represents model bathymetry and topography (m), where negative values denote seafloor depth and positive values denote land elevation.

The simulation results indicate pronounced spatial variability in tsunami characteristics along the southern coast of East Java, including tsunami arrival time, wave amplitude, and current velocity. These variations reflect differences in coastal exposure, bathymetry, and nearshore geomorphology at each VTG location.

At Pancer Beach, Jember, the first significant tsunami wave arrived approximately 0.4 hours (±24 minutes) after the initial seafloor deformation, preceded by an initial sea-level drawdown. Wave amplitudes ranged from approximately +12 m to −15 m, representing the highest oscillations among the VTGs. Maximum horizontal current velocities reached about 3–4 m/s, indicating high destructive potential capable of causing severe structural damage and increased risk to coastal populations [38].

At the Nusa Barung VTG, the tsunami arrived slightly earlier, at about 0.35 hours (±21 minutes), but with lower amplitudes of approximately +7 m to -5 m. The reduced wave energy is interpreted as an island shielding effect, where Nusa Barung Island partially obstructs tsunami propagation from the south. Correspondingly, lower maximum current velocities of around 1.2 m/s suggest a comparatively reduced hazard level relative to adjacent open-coast locations.

Watu Gedek Beach, Lumajang, experienced the first tsunami arrival at approximately 0.45 hours (±27 minutes), with wave amplitudes reaching +12 m and -8 m. Maximum current velocities of about 3 m/s indicate strong tsunami flow conditions, which may contribute to coastal structural damage and significant sediment transport.

At Lampon Beach, Banyuwangi, the tsunami arrival time was also approximately 0.45 hours (±27 minutes). Wave amplitudes were relatively lower, ranging from about +4 m to -3 m, indicating weaker vertical oscillation compared with the other VTG locations. Maximum horizontal current velocities reached about 1 m/s, suggesting that hazard characteristics at this site are associated more with sustained coastal currents and localized erosion processes rather than extreme wave impact. This behavior may reflect local bathymetric control and partial energy dissipation before coastal arrival [26-27].

These results are consistent with observations from the 1994 Banyuwangi tsunami, where reported run-up heights ranged from approximately 4 m to 14 m at several coastal locations, including Lampon and surrounding areas, as documented by field surveys [8],[39]. It should be noted that VTG amplitudes represent nearshore water-level fluctuations and are not directly equivalent to onshore run-up heights. Run-up values are typically higher due to coastal amplification processes [26-27]. These findings further highlight the importance of considering both wave height and flow velocity in tsunami hazard assessment [38],[40].

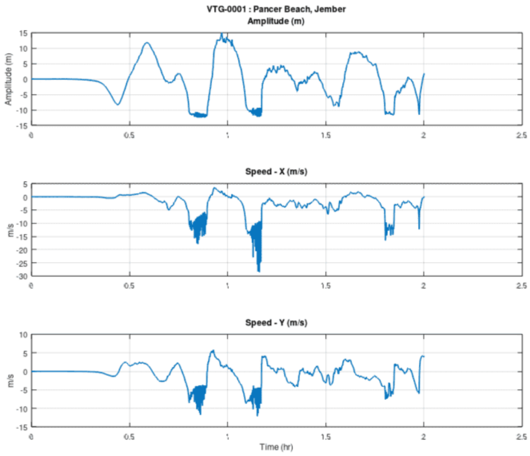

(a) Pantai Pancer Jember

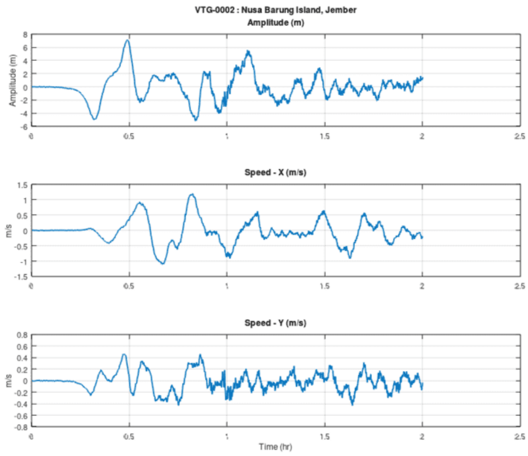

(b) Pulau Nusa Barung Jember

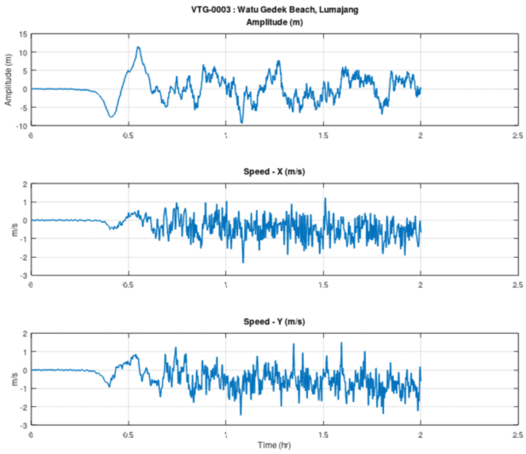

(c) Pantai Watu Gedek Lumajang

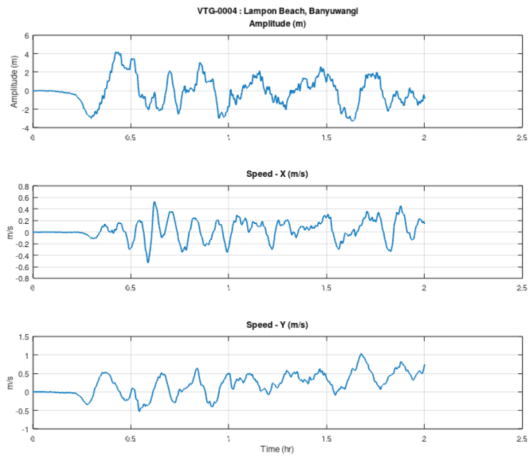

(d) Pantai Lampon Banyuwangi

Figure 8. Simulated time series of tsunami water surface elevation (Amplitude, m) and horizontal current velocities (Speed-X and Speed-Y, m/s) at four Virtual Tsunami Gauge (VTG) locations along the southern coast of East Java: (a) Pancer Beach, Jember; (b) Nusa Barung Island, Jember; (c) Watu Gedek Beach, Lumajang; and (d) Lampon Beach, Banyuwangi.

Overall, the VTG analysis reveals distinct dominant hazard characteristics at each site. Pancer Beach and Watu Gedek are primarily affected by high tsunami wave amplitudes, whereas Lampon Beach appears to be influenced more by moderate coastal current dynamics and localized erosion potential than by extreme wave impact. These results highlight the importance of considering both wave height and flow velocity when assessing tsunami hazard variability along the southern coast of East Java. The key simulation parameters derived from the VTG analysis are summarized in Table 2 to support the spatial comparison of tsunami hazard levels across the study area.

Table 2. Summary of tsunami simulation parameters at four Virtual Tsunami Gauges (VTGs), including tsunami arrival time, maximum and minimum wave amplitudes, and maximum current velocities in the X and Y directions. Dominant Hazard Characteristics

VTG Location	Arrival Time (hours)	Max Amp. (m)	Min Amp. (m)	Vmax X (m/s)	Vmax Y (m/s)	Dominant Hazard Characteristics
Pancer Beach - Jember	~0.4	+12	-14	~3	~4	Very high tsunami waves, high destructive potential
Nusa Barung - Jember	~0.35	+7	-5	~1.2	~0.7	Island shielding effect, prolonged secondary waves
Watu Gedek - Lumajang	~0.45	+12	-8	~3	~2	Strong wave energy, combined wave and current hazard
Lampon Beach - Banyuwangi	~0.45	+4	-3	~0.5	~1.0	Moderate currents, localized erosion potential

Tsunami Hazard Map

The tsunami inundation depth map (Estimated Tsunami Height/ETH) shown in Figure 9 indicates that Puger Kulon Village represents the area with the highest tsunami hazard level under the southern East Java megathrust tsunami scenario. The village is located on an open coastal plain directly facing the Indian Ocean and adjacent to the Puger River mouth, which functions as a primary pathway for tsunami waves to penetrate inland [36-37]. The relatively flat topography further enhances wave intrusion, allowing inundation to extend deeply into residential areas [14],[40].

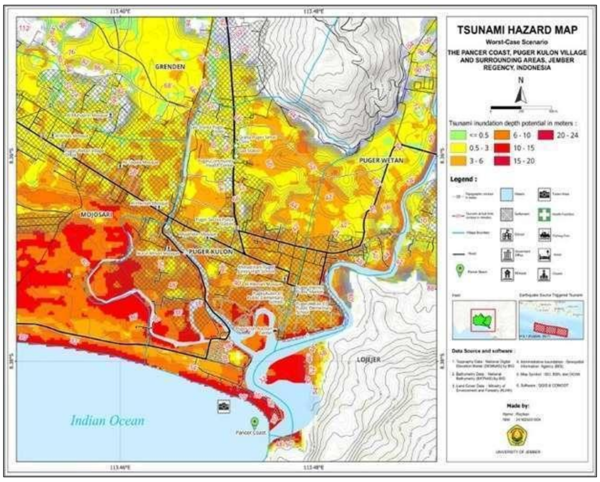

Figure 9. Tsunami hazard map showing estimated tsunami height (ETH, represented by the color legend) and estimated tsunami arrival time (ETA, represented by numerical labels in minutes) in the Pancer–Puger Kulon coastal area, Jember.

The inundation pattern in Puger Kulon is predominantly characterized by ETH classes of 6–20 m, represented by orange to red colors, while several localized coastal hotspots exhibit extreme values exceeding 20 m. This spatial pattern is consistent with the Virtual Tsunami Gauge (VTG) analysis, which identified large wave amplitudes and high current velocities along exposed coastal sectors. River channels, flat residential zones, and agricultural land act as natural corridors for tsunami propagation, enabling inundation to advance further inland.

The integration of the ETH distribution and the estimated Time of Arrival (ETA) further emphasizes the hazard level in Puger Kulon. The first tsunami wave is estimated to arrive within approximately 20–24 minutes, indicating not only deep inundation but also a very limited evacuation time compared to surrounding villages [14],[41]. The combination of high inundation depth and rapid wave arrival places Puger Kulon as the area with the highest tsunami risk within the study region.

Other villages, including Mojosari, Mojomulyo, Puger Wetan, Grenden, and Lojejer, are also included in the hazard map to provide a comprehensive spatial overview. However, those areas generally exhibit lower inundation depths and slightly longer arrival times, primarily influenced by higher local topography, vegetation cover, and greater distances from the shoreline.

An overlay analysis between the ETH map and village administrative boundaries provides an estimate of tsunami-affected areas across five coastal villages in Puger District, as summarized in Table 3. The results show that Puger Kulon experiences inundation over approximately 5.267 km^2, accounting for about 97.95% of the total village area, with inundation depths predominantly ranging from 6 to 20 m. Mojosari Village exhibits similarly extreme exposure, with inundation covering 9.782 km^2 or 99.85% of its total area, reflecting the high vulnerability of low-lying terrain directly connected to tsunami propagation pathways.

Table 3. Inundation area and percentage by tsunami depth classes (ETH) for Puger Kulon and surrounding villages.

No	Village Name	Inundated Area (km²) based on ETH Class						Total Inundated Area (km²)	Village Area (km²)	Percent Inundated area
		(0.5–3) m	(3–6) m	(6–10) m	(10–15) m	(15–20) m	(20–24) m			
1.	Puger Kulon	0.047	0.521	2.092	1.958	0.578	0.071	5.267	5.377	97.95
2.	Puger Wetan	0.167	1.133	1.055	0.291	0.140		2.786	5.363	51.95
3.	Mojosari	0.226	2.421	2.742	1.865	2.528		9.782	9.797	99.85
4.	Grenden	0.723	2.327	0.241	0.030			3.321	12.243	27.13
5.	Mojomulyo	0.346	2.539	1.901	2.295	1.212	0.108	8.401	9.684	86.75

In contrast, Puger Wetan experiences moderate inundation (51.95%), dominated by low to intermediate depths, while Mojomulyo shows a high inundation level (86.75%). Grenden Village displays relatively low exposure (27.13%), which is associated with higher topography and greater distance from the coastline. Overall, these results confirm that Puger Kulon and Mojosari constitute the two highest-risk areas in terms of both inundation extent and depth, and therefore should be prioritized in tsunami mitigation planning and disaster-resilient spatial development along the southern coast of Jember Regency, consistent with previous tsunami hazard assessments in southern Java [5].

CONCLUSION

The tsunami modeling results based on a worst-case Mw 8.7 megathrust earthquake scenario south of East Java indicate that the Puger coastal area, particularly Puger Kulon and Mojosari villages, exhibits the highest level of tsunami hazard. Numerical simulations using COMCOT with a five-level nested grid configuration successfully represent the processes of tsunami generation, propagation, and inundation, and capture spatial variations in coastal wave response through Virtual Tsunami Gauge (VTG) analysis. Both villages experience extensive inundation, with dominant depths ranging from 6–20 m and localized areas exceeding 20 m, consistent with the large wave amplitudes and strong current velocities observed in the VTG results.

In contrast, Puger Wetan, Mojomulyo, and Grenden villages show relatively lower tsunami impacts, mainly due to higher local topography and greater distance from the primary tsunami propagation pathways. The integration of tsunami inundation depth (ETH) and estimated tsunami arrival time (ETA) demonstrates that open coastal plains represent the highest-risk zones, as they are characterized by both deep inundation and very limited evacuation time.

These findings highlight the urgent need to prioritize tsunami mitigation efforts in Puger Kulon and Mojosari, particularly through improved evacuation planning, risk-informed spatial planning, and the strengthening of tsunami early warning systems. Given the short arrival time (approximately 21–27 minutes) and high inundation levels, the implementation of tsunami vertical evacuation shelters, such as elevated reinforced structures or multi-story buildings located near densely populated coastal areas, is considered a practical and realistic mitigation strategy. This approach should be supported by well-defined evacuation routes, community preparedness programs, and regular evacuation drills to enhance the effectiveness of tsunami risk reduction in the study area.

ACKNOWLEDGMENTS

The authors would like to express their sincere gratitude to the Geophysics Station of Pasuruan, Indonesian Agency for Meteorology, Climatology, and Geophysics (BMKG), for the support, data assistance, and valuable technical insights provided during this research. The authors also extend their appreciation to all parties who contributed through discussions and technical support throughout the numerical modeling and analysis process.

REFERENCES

[1] Hall, R. (2011). Australia–SE Asia collision: Plate tectonics and crustal flow (Vol. 355). https://doi.org/10.1144/SP355.5

[2] Simons, W. J. F., Socquet, A., Vigny, C., Ambrosius, B. A. C., Haji Abu, S., Promthong, C., Subarya, C., Sarsito, D. A., Matheussen, S., Morgan, P., & Spakman, W. (2007). A decade of GPS in Southeast Asia: Resolving Sundaland motion and boundaries. Journal of Geophysical Research: Solid Earth, 112(6). https://doi.org/10.1029/2005JB003868

[3] Pusat Studi Gempa Nasional (PuSGeN). (2017). Pusat Penelitian dan Pengembangan Perumahan dan Permukiman (Indonesia).

[4] Widiyantoro, S., Gunawan, E., Muhari, A., Rawlinson, N., Mori, J., Hanifa, N. R., Susilo, S., Supendi, P., Shiddiqi, H. A., & Nugraha, A. D. (2022). Seismic structure and megathrust segmentation beneath Java. Geophysical Journal International, 229(2), 1095–1112. https://doi.org/10.1093/gji/ggab501

[5] Widiyantoro, S., Gunawan, E., Rosalia, S., & others. (2020). Implications of the morphostructure of the southern Java subduction zone for megathrust potential. Marine Geology, 430, 106328.

[6] Gusman, A. R., & Tanioka, Y. (2017). Tsunami generation by megathrust earthquakes along the Java trench. Pure and Applied Geophysics, 174, 317–332. https://doi.org/10.1007/s00024-016-1425-8

[7] Muhari, A., & Imamura, F. (2018). Historical tsunami records and hazard assessment in Indonesia. Journal of Disaster Research, 13(2), 293–304. https://doi.org/10.20965/jdr.2018.p0293

[8] Tsuji, Y., Imamura, F., Matsutomi, H., Synolakis, C. E., Nanang, P. T., Jumadi, Harada, K., Han, S. S., & Aoyama, M. (1995). Field survey of the East Java earthquake and tsunami of June 3, 1994. Pure and Applied Geophysics PAGEOPH, 144(3–4). https://doi.org/10.1007/BF00874397

[9] Muhari, A., Imamura, F., Arikawa, T., Hakim, A. R., & Afriyanto, B. (2020). Tsunami risk reduction strategies in Indonesia. International Journal of Disaster Risk Reduction, 49, 101660. https://doi.org/10.1016/j.ijdrr.2020.101660

[10] Bupati Kabupaten Jember. (2015). Perda Kabupaten Jember No. 1 Tahun 2015 tentang RTRW Kabupaten Jember Tahun 2015–2035. Perda, 1–138.

[11] Badan Nasional Penanggulangan Bencana. (2023). Risiko Bencana Indonesia "Memahami Risiko Sistemik di Indonesia." Retrieved from https://inarisk.bnpb.go.id/BUKU-RBI-2022/mobile/index.html#p=10

[12] BNPB. (2024). InaRISK Dashboard: Peta Risiko Tsunami Jawa Timur Tahun 2024.

[13] Suppasri, A., & Koshimura, S. (2016). Characteristics of tsunami hazard and risk in coastal areas. Natural Hazards, 84, 183–204. https://doi.org/10.1007/s11069-016-2459-3

[14] Løvholt, F., Glimsdal, S., Harbitz, C. B., Zamora, N., Nadim, F., Peduzzi, P., & others. (2019). Global tsunami hazard and exposure. Nature Communications, 10, 180. https://doi.org/10.1038/s41467-018-08238-5

[15] Hanifa, N. R., Latief, H., Nugroho, S. P., & Meilano, I. (2018). Potential tsunami hazards due to megathrust earthquake along Java trench: Numerical modeling approach. IOP Conference Series: Earth and Environmental Science, 162, 012016. https://doi.org/10.1088/1755-1315/162/1/012016

[16] Imamura, F., & Koshimura, S. (2020). Recent developments of tsunami simulation and disaster mitigation. Annual Review of Earth and Planetary Sciences, 48, 111–139.

[17] Wang, X., & Power, W. L. (2011). COMCOT: A tsunami generation propagation and run-up model.
[18] Widada, S., Darda, I. M., & Satriadi, A. (2022). Identifikasi wilayah terdampak tsunami berdasarkan peta ancaman tsunami di Kabupaten Lumajang, Jawa Timur. Buletin Oseanografi Marina, 11(3). https://doi.org/10.14710/buloma.v11i3.44032
[19] Wang, X., & Liu, P. L.-F. (2016). COMCOT tsunami modeling framework. Journal of Marine Science and Engineering, 4(2), 30. https://doi.org/10.3390/jmse4020030
[20] Liu, P. L.-F., Lynett, P., Fernando, H., Jaffe, B. E., Fritz, H., Higman, B., Morton, R., Goff, J., & Synolakis, C. (2018). Advances in numerical tsunami modeling. Annual Review of Fluid Mechanics, 50, 609–634. https://doi.org/10.1146/annurev-fluid-122316-045009

[21] Suppasri, A., & Imamura, F. (2018). Tsunami modeling and evacuation planning. Coastal Engineering Journal, 60(2), 198–215. https://doi.org/10.1080/21664250.2018.1436903
[22] Koshimura, S., Suppasri, A., Namegaya, Y., & Imamura, F. (2019). Probabilistic tsunami hazard and risk assessment. Coastal Engineering, 152, 103527. https://doi.org/10.1016/j.coastaleng.2019.103527
[23] Weatherall, P., Marks, K. M., Jakobsson, M., Schmitt, T., Tani, S., Arndt, J. E., Ryder, C., Wigley, R., Ferrini, V., & others. (2015). A new digital bathymetric model of the world's oceans. Earth and Space Science, 2(8), 331–345.
[24] Badan Informasi Geospasial (BIG). (2018). DEMNAS (Digital Elevation Model Nasional). Cibinong, Indonesia.
[25] Chow, V. T. (1959). Open-channel hydraulics. New York: McGraw-Hill Book Company.
[26] Setyonegoro, W. (2022). Pengaruh gaya gesek dan tekanan hidrostatik pada propagasi tsunami (Studi kasus: Jawa Timur 3 Juni 1994). Buletin Meteorologi, Klimatologi, dan Geofisika, 2(4), 18–41.
[27] Satake, K. (2014). Advances in earthquake and tsunami sciences and disaster risk reduction since the 2004 Indian Ocean tsunami. Geoscience Letters, 1. https://doi.org/10.1186/s40562-014-0015-7
[28] Wells, D. L., & Coppersmith, K. J. (1994). New empirical relationships among magnitude, rupture length, rupture width, rupture area, and surface displacement. Bulletin of the Seismological Society of America, 84(4), 974–1002.
[29] Kanamori, H. (1977). The energy release in great earthquakes. Journal of Geophysical Research, 82(20), 2981–2987.
[30] Okada, Y. (1985). Surface deformation due to shear and tensile faults in a half-space. Bulletin of the Seismological Society of America, 75(4), 1135–1154. https://doi.org/10.1785/BSSA0750041135
[31] Liu, P., Wang, X., & Salisbury, A. (2009). Tsunami hazard and early warning system in South China Sea. Journal of Asian Earth Sciences, 36, 2–12. https://doi.org/10.1016/j.jseaes.2008.12.010
[32] Wang, X., & Liu, P. L.-F. (2006). An analysis of 2004 Sumatra earthquake fault plane mechanisms and Indian Ocean tsunami. Journal of Hydraulic Research, 44(2), 147–154.
[33] Ratnasari, R. N., Tanioka, Y., & Gusman, A. R. (2020). Determination of source models appropriate for tsunami forecasting: Application to tsunami earthquakes in Central Sumatra, Indonesia. Pure and Applied Geophysics, 177(6), 2551–2562. https://doi.org/10.1007/s00024-020-02483-3
[34] Setyonegoro, W. (2022). Pengaruh gaya gesek dan tekanan hidrostatik pada propagasi tsunami (Studi kasus: Tsunami Jawa Timur 3 Juni 1994). Buletin Meteorologi, Klimatologi, dan Geofisika, 3(3), 18–41.
[35] Lay, T., Kanamori, H., Ammon, C. J., Nettles, M., Ward, S. N., Aster, R. C., Beck, S. L., Bilek, S. L., Brudzinski, M. R., Butler, R., DeShon, H. R., Ekström, G., Satake, K., & Sipkin, S. (2005). The great Sumatra-Andaman earthquake of 26 December 2004. Science, 308(5725), 1127–1133. https://doi.org/10.1126/science.1112250
[36] Widiyantoro, S., Gunawan, E., Muhari, A., Rawlinson, N., Supendi, P., & Ash Shiddiqi, H. (2020). Implications for megathrust earthquakes and tsunamis from seismic gaps south of Java Indonesia. Scientific Reports, 10. https://doi.org/10.1038/s41598-020-72142-z

[37] Koshimura, S., Namegaya, Y., & Yanagisawa, H. (2009). Tsunami fragility – A new measure to identify tsunami damage –. Journal of Disaster Research, 4(6), 479–488. https://doi.org/10.20965/jdr.2009.p0479

[38] Suppasri, A., Mas, E., Charvet, I., Gunasekera, R., Imai, K., Fukutani, Y., Abe, Y., & Imamura, F. (2013). Building damage characteristics based on surveyed data and fragility curves of the 2011 Great East Japan tsunami. Natural Hazards, 66(2), 319–341. https://doi.org/10.1007/s11069-012-0487-8

[39] Fritz, H. M., Borrero, J. C., Synolakis, C. E., & Yoo, J. (2006). 2004 Indian Ocean tsunami flow velocity measurements from survivor videos. Geophysical Research Letters, 33(24), L24605. https://doi.org/10.1029/2006GL026784

[40] Nugraha, H. A., & Pandadaran, S. H. (2024). Katalog Tsunami Indonesia Tahun 416–2023 Per-Wilayah.

[41] Synolakis, C. E., Bernard, E. N., Angeles, L., & Marine, P. (2006). Tsunami science before and beyond Boxing Day 2004. Philosophical Transactions of the Royal Society A, 364(1845), 2231–2265. https://doi.org/10.1098/rsta.2006.1824